JOURNAL OF GEOPHYSICAL RESEARCH, VOL. 108, NO. A12, 1415, doi:10.1029/2003JA009865, 2003

Modification of the solar wind electron velocity distribution at interplanetary shocks

R. J. Fitzenreiter and K. W. Ogilvie
Nasa Goddard Space Flight Center, Greenbelt, Maryland, USA

S. D. Bale
Space Sciences Laboratory, University of California, Berkeley, Berkeley, California, USA

A. F. Viñas
NASA Goddard Space Flight Center, Greenbelt, Maryland, USA

Received 29 January 2003; revised 20 August 2003; accepted 29 August 2003; published 2 December 2003.

[1] We analyze a small selection of interplanetary shocks of moderate strength, observed by instruments aboard the Wind spacecraft. We find electron signatures of heating and acceleration that are similar to those found at Earth's high Mach number bow shock. Upstream, velocity distributions have the signature of shock-accelerated electrons with the characteristic time of flight velocity cutoff with bump-on-tail reduced distributions observed in coincidence with Langmuir waves. Downstream, the distributions broaden with the stronger shocks showing flat-topped distributions and accompanying beams, such as are seen on the high entropy side of Earth's bow shock. We apply the Liouville mapping analysis of *Hull et al.* [1998, 2001] to one of the interplanetary shocks and compute the deHoffman-Teller electrostatic potential across the shock using the electron moments to map the observed upstream distribution to the downstream region. The mapping successfully reproduces the inflated phase density and beam signatures of the observed downstream electron velocity distribution. *INDEX TERMS:* 2139 Interplanetary Physics: Interplanetary shocks; 2164 Interplanetary Physics: Solar wind plasma; 7815 Space Plasma Physics: Electrostatic structures; 7807 Space Plasma Physics: Charged particle motion and acceleration; *KEYWORDS:* solar wind electrons, interplanetary shock

Citation: Fitzenreiter, R. J., K. W. Ogilvie, S. D. Bale, and A. F. Viñas, Modification of the solar wind electron velocity distribution at interplanetary shocks, *J. Geophys. Res.*, *108*(A12), 1415, doi:10.1029/2003JA009865, 2003.

1. Introduction

[2] We report the observation and analysis of solar wind electron distributions at several interplanetary shocks using particle and field data from the Wind spacecraft. As a shock sweeps through the solar wind, it modifies the distribution function of electrons and ions in its path. Electrons with their relatively low inertia when compared with the ions are fully magnetized and behave adiabatically, executing helical trajectories in the shock magnetic and electric fields [e.g., *Goodrich and Scudder*, 1984; *Scudder*, 1995]. The shock electric field is often characterized by the electric potential in the deHoffman-Teller frame, which is the shock frame that moves along the shock surface such that the convection electric field ($\mathbf{V_{SW}} \times \mathbf{B}$) is zero on both sides of the shock. In this frame the electrons experience only the magnetic ramp of the shock and the remaining cross-shock electric field. Electrons with pitch angles less than the mirror loss-cone angle spiral through these fields gaining kinetic energy equal to the deHoffman-Teller electric potential.

[3] There have been relatively few published three-dimensional (3-D) observations of electron velocity distributions at interplanetary shocks [*Bale et al.*, 1999; *Feldman et al.*, 1983b]. Measurements of electron distributions across interplanetary shocks were used by *Feldman et al.* [1983b, 1983c] to study electron heating by the shock. They found that for weaker shocks, the electron heating was primarily perpendicular to the magnetic field, consistent with the conservation of magnetic moment of electrons passing through the shock to the higher magnetic field intensity region downstream. For stronger, intermediate strength shocks, flat-topped distributions were observed downstream, similar to those observed at the Earth's bow shock, and parallel heating was dominant. Feldman et al. suggested that the shock associated electric field accounted for the parallel electron heating. The stronger, intermediate strength shocks in the Feldman et al. study had downstream to upstream density ratios in the range between 2 and 4. The interplanetary shocks in the current study are also of intermediate strength with downstream to upstream density ratios between 2.4 and 3.9, and all exhibit both parallel and

0148-0227/03/2003JA009865$09.00

Table 1. Observed Characteristics of Interplanetary Shocks

Date	UT	B_2/B_1	Te_2-Te_1 eV	Ne_2/Ne_1	M_A	θ_{bn} deg	V_{shock} km/s	U_{sw1} km/s	Shock Normal **n**	Flattop Down-stream	Beam on Flattop	Upstream Electrons, Waves
26 Aug 1998	0640	3.11	41.6	3.4	6.4	67	602	474	(−0.474, 0.264, −0.840)	Yes	Yes	Yes
10 Nov 2000	0619	2.99	30.7	3.9	2.9	83	873	644	(−0.926, −0.244, 0.288)	Yes	Yes	No
18 Feb 1999	0249	2.91	17.3	2.5	4.1	55	712	412	(−0.995, −0.095, −0.023)	Yes	No	Yes
6 Apr 2000	1627	2.85	22.8	3.0	2.0	84	376	380	(−0.697, −0.273, 0.663)	Yes	No	Yes
21 Oct 1999	0213	2.58	4.3	3.0	2.4	76	475	356	(−0.982, −0.044, 0.019)	No	No	No
15 May 1997	0115	2.38	8.4	2.4	3.8	85	417	320	(−0.826, −0.457, −0.330)	No	No	Yes

perpendicular electron heating. The flat-topped distributions of the two strongest shocks also have prominent downstream beams aligned with the magnetic field, similar to those observed downstream at the Earth's bow shock [*Feldman et al.*, 1983a]. To our knowledge, this is the first observation of downstream electron beams associated with interplanetary shocks. We use the Liouville mapping technique first used by *Hull et al.* [1998, 2001], in which the full velocity distribution function upstream of the shock is mapped through the magnetic field and electrostatic potential at the shock layer to the downstream region. We restrict our comparison of the mapped distribution with the downstream flat-topped distribution to those phase space regions that are accessible to upstream electrons. The flattop phase space region is inaccessible to upstream electrons and must be determined by other means, such as filling in via scattering, and is not part of this study. In the accessible downstream phase space region, the mapping successfully reproduces the observed parallel and perpendicular inflation in phase space density, consistent with electron heating, as well as the beam at the edge of the flattop.

2. Observations

[4] Data from five instruments on board the Wind spacecraft have been used in this study. The vector magnetic field data are the 3 s measurements from the Magnetic Field Investigation (MFI) [*Lepping et al.*, 1995] and the plasma wave measurements are from the Thermal Noise Receiver of the WAVES experiment [*Bougeret et al.*, 1995]. The ion density and flow velocity are derived from the Faraday cup of the Solar Wind Experiment (SWE) [*Ogilvie et al.*, 1995] at the rate of one measurement per 96 s. The SWE Vector Electron Ion Spectrometer (VEIS) measures 3-D electron velocity distributions over a 3 s spin period once each 12 s and the electron density and electron temperature are derived from moment integrals over the velocity distributions. The lowest energy measurement of the velocity distribution is 13 eV, which means that the breakpoint measurement of the spacecraft potential cannot generally be made in the solar wind. Therefore an estimate for the spacecraft potential correction to the measured electron velocity distribution is determined by an iterative procedure in which the potential is computed using the ratio of the initially determined electron moment density to the measured ion density and the assumption of charge neutrality between the electrons and ions. A fitted Gaussian is used to represent the core of the electron distribution below 13 eV. Since the Faraday cup density measurement used in this study only includes protons, a 10% correction is added as an estimate for the doubly ionized helium contribution to the solar wind ions. The measured electron velocities are then corrected using the estimated spacecraft potential and the moments are recomputed resulting in a final electron density, temperature, and heat flux. For the purpose of the spacecraft potential estimate, the lower time resolution Faraday cup measurements are interpolated on the higher resolution VEIS measurement times. All electron moment and distribution function data used in this paper have been corrected using the estimated spacecraft potential determined in this way.

2.1. Overview

[5] We present observations of a set of six quasi-perpendicular fast-forward interplanetary shocks, which were chosen for data quality and suitability for analysis. A summary of the properties of the interplanetary shocks included in this study is given in Table 1. Throughout this paper, the subscripts 1 and 2 of the plasma parameters refer to upstream and downstream of the shock, respectively. The shocks are listed in Table 1 in order of the downstream to upstream magnetic field intensity ratio, B_2/B_1. Also listed are the shock strength, given by the electron density ratio, Ne_2/Ne_1, the Alfvén Mach number, M_A, and the electron temperature increase across each shock, Te_2-Te_1, in units of eV. A Rankine-Hugoniot (R-H) analysis was applied to each shock using the SDAT (Shock Discontinuities Analysis Tool), which is a tool based on the Viñas-Scudder method [*Viñas and Scudder*, 1986]. The analysis determines the shock normal, **n**, which points toward the upstream side of the shock, and the shock speed in the spacecraft frame, v_{shock}, along **n**. The shock normal **n**, the angle θ_{Bn}, v_{shock}, and u_{sw1} are tabulated, where θ_{Bn} is the angle between the upstream magnetic field $\mathbf{B}_1$ and the shock normal **n**. These shocks were all quasi-perpendicular, with an average value $\langle\theta_{Bn}\rangle = 72°$.

[6] Figure 1 illustrates the passage of one of the strongest interplanetary shocks, 26 August 1998. The electron density measured by the VEIS and the ion density measured by the Faraday cup are plotted together in the top panel and show the different time resolutions of the electron and ion measurements as discussed above. The electron temperature, the ion flow speed, and the 3 s resolution magnetic field magnitude are plotted in the second, third, and fourth panels from the top, respectively. The shock is identified by the jump in density, flow speed, electron temperature, and magnetic field intensity which occurs between 0640 and 0641 UT. The bottom panel is the counts spectrum summed over all angles measured by VEIS over the energy range 13 eV to 973 eV, plotted on the vertical axis. It can be seen that the peak of the electron counts distribution increases in energy across the shock from 40 eV to 120 eV, approximately, and increases almost tenfold in counting rate.

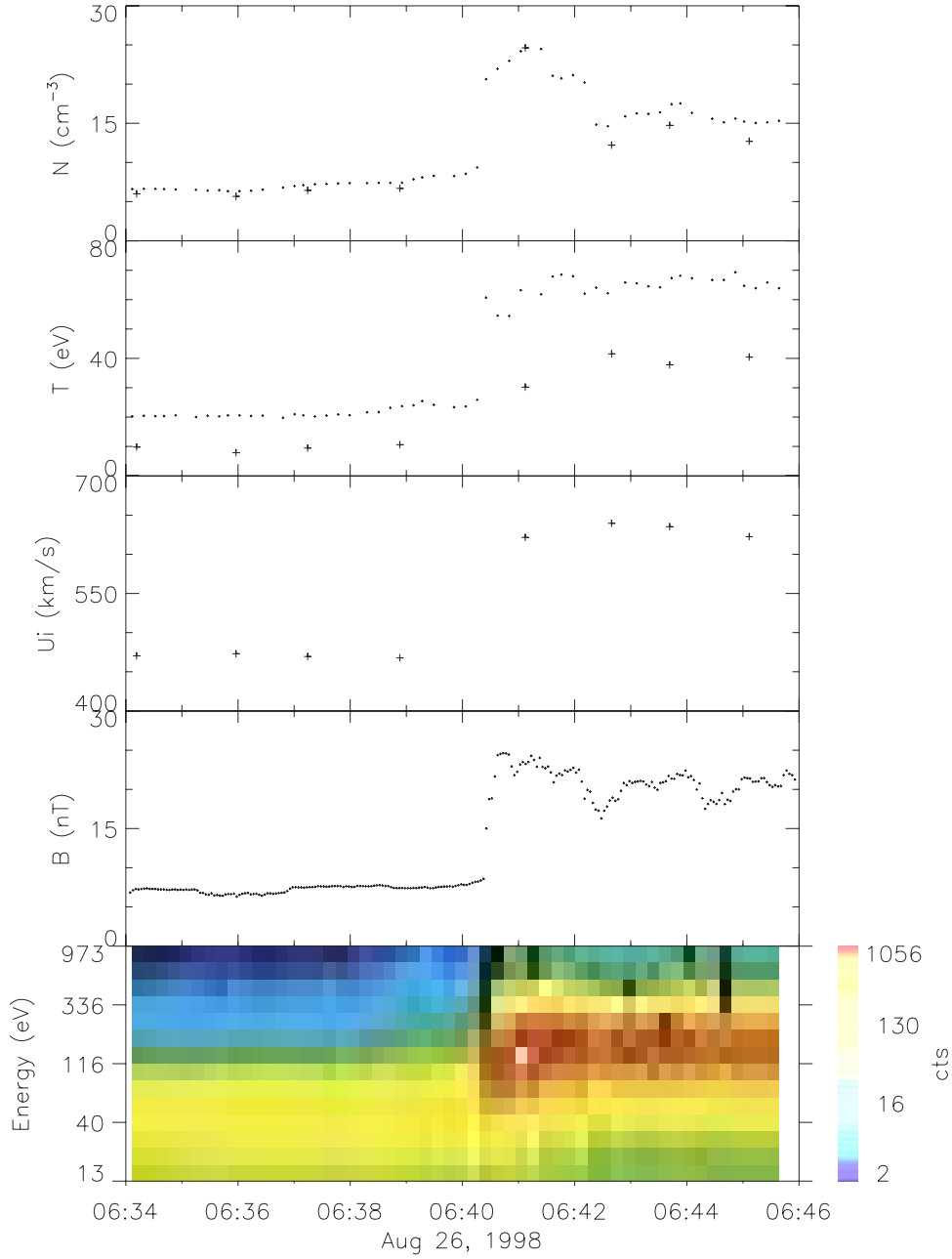

Figure 1. An overview of the passage of the interplanetary shock past the Wind spacecraft on 26 August 1998. The top two panels are the solar wind plasma density and temperature, respectively, with the electron density and temperature plotted as dots, and the lower resolution ion density and temperature plotted as "plus" symbols. The solar wind speed is plotted in the third panel and the 3s magnetic field intensity is plotted in the fourth panel. The bottom panel is the electron counts spectrum summed over angle as a function of energy. The shock transition occurs between 0640 and 0641.

[7] The shock passages of four of the interplanetary shocks, 26 August 1998, 10 November 2000, 18 February 1999, and 15 May 1997, are illustrated on expanded time scales in Figure 2. For each shock, the top four panels are the same as in Figure 1, while the bottom panel shows the WAVES/TNR measurements of the electric field fluctuations. For three of the shocks (plotted in Figure 2a, 2c, and 2d), plasma line enhancements upstream of the shock indicate Langmuir wave generation by electrons accelerated upstream by the shock and will be discussed later in this section.

2.2. Downstream Heating and Acceleration of Electrons

[8] Figure 3a–3d shows the electron velocity distributions both upstream and downstream of each of the four shocks in Figure 2. Pitch angle distributions have been computed from the measured velocity distributions trans-

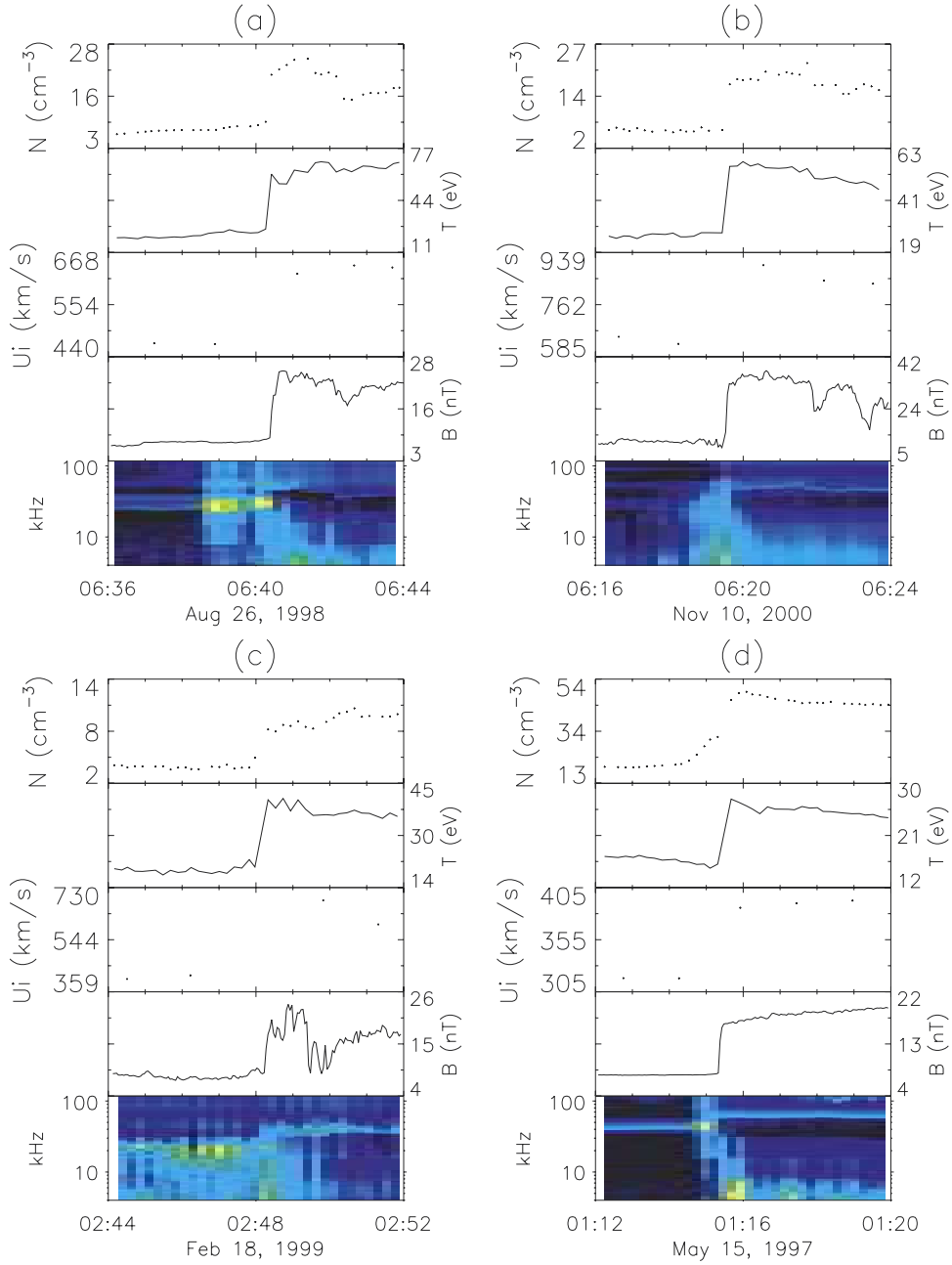

Figure 2. Measurements of the upstream to downstream transition for four of the six interplanetary shocks included in this study. Beginning at the top panel for each shock, the data plotted are the electron density, electron temperature, solar wind speed, magnetic field intensity, and electric field fluctuations from the WAVES/TNR experiment. Electron heating by the shock is indicated by the rise in electron temperature. The upstream enhancements in the electric field fluctuations in Figures 2a, 2c, and 2d show that Langmuir waves are generated in the foreshock region upstream of interplanetary shocks similar to the electron foreshock of Earth's bow shock.

formed to the solar wind frame and are plotted in the upper panels as contours on the velocity grid, parallel and perpendicular to the magnetic field, and the cuts parallel (solid curve) and perpendicular (dashed curve) are plotted in the lower panels. The triangular points are the measurements closest to the parallel and antiparallel directions. The dotted curves are the computed one-count levels. Comparison of the upstream and downstream distributions for each of the four shocks shown in Figure 3 shows that electron heating across the shock broadens the distributions both parallel and perpendicular to the magnetic field. These four shocks were chosen because they cover the range of electron heating available in our data set. Flat-topped distributions can be seen in three cases, 26 August 1998, 10 November 2000, and 18 February 1999, and are similar to distributions observed downstream of the Earth's bow shock [*Feldman et al.*, 1983a] and to those downstream of intermediate strength interplanetary shocks [*Feldman et al.*, 1983b]. The

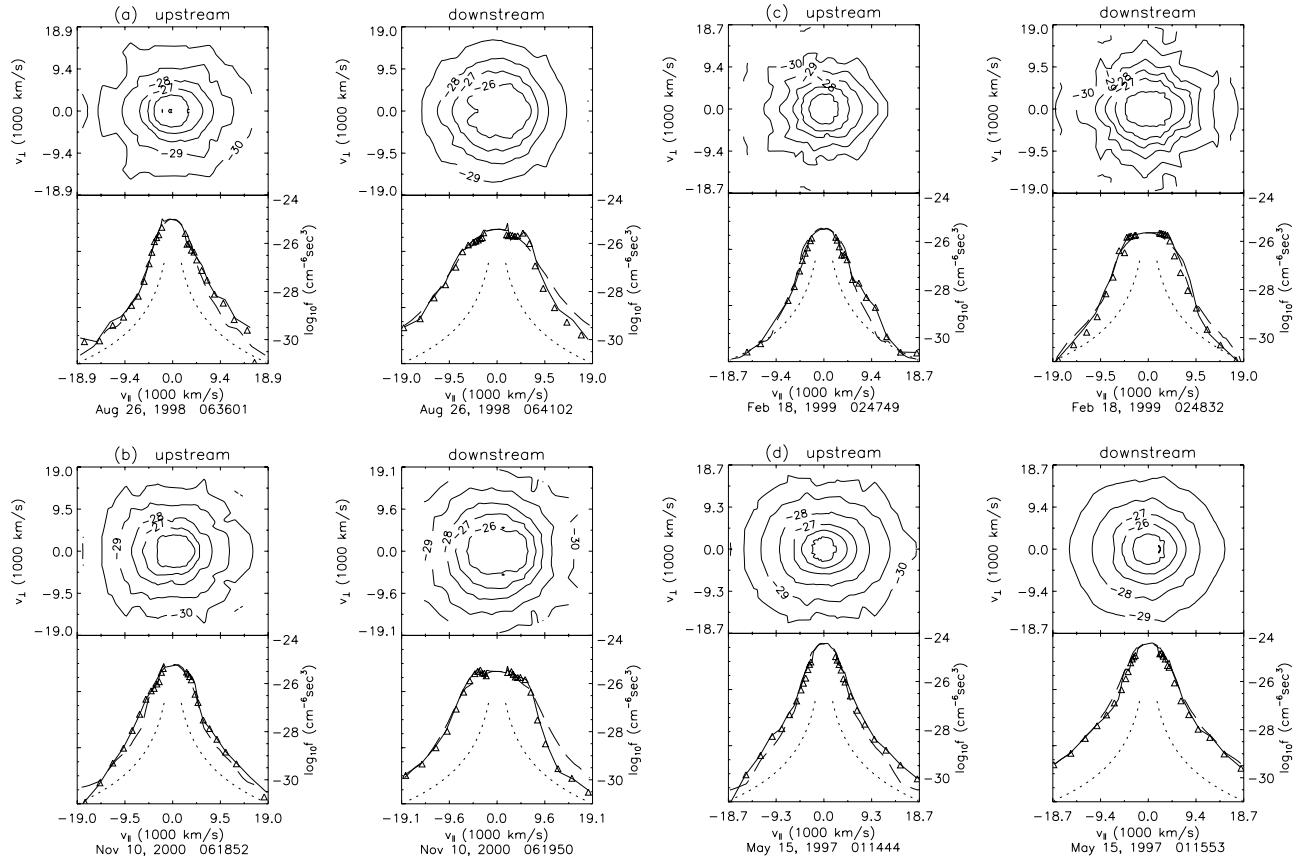

Figure 3. The electron velocity distributions measured upstream and downstream of each of the four shocks included in Figure 2. Comparison of the downstream and upstream distributions shows that as indicated by the inflation of the downstream distributions, the shock transition results in electron heating in both the parallel and perpendicular directions. The shocks in Figures 3a through 3d are ordered according to decreasing amount of electron heating.

parallel cuts of the two strongest shocks in Figure 3a and 3b each have a beam at a speed of approximately 5000 km/s which is directed toward the downstream side in each case. These beams are shown in greater detail in Figure 4, which shows the low velocity range of the distributions in Figure 3a and 3b. The location of each measurement in velocity space is shown as a point underlying the contours. The beams are evident in the parallel cuts and by the closed contours located at +5000 km/s in the 26 August 1998 case and at −5000 km/s in the 10 November 2000 case. It is clear that the existence of the beams is well supported by the data samples within the closed contours and by the ratio of the cuts, $f_{\|}/f_{\perp}$, being significantly >1 in the vicinity of the beams. To show that these beams are directed downstream, we compare the downstream magnetic field vector, $\mathbf{B}_2$, with the shock normal, **n**, which points upstream in all cases. For the 26 August 1998 shock in Figure 3a, **n** = [−0.474, 0.264, −0.840], $\mathbf{B}_2$ = [−12.82, 13.67, 13.17], and $\mathbf{n}\bullet\mathbf{B}_2 = -1.38$; $\mathbf{B}_2$ has a component opposing **n** and therefore the beam along $+\mathbf{B}_2$ is directed toward the downstream side. For the 10 November 2000 shock in Figure 3b, **n** = [−0.926, −0.244, 0.288], $\mathbf{B}_2$ = [3.46, −16.81, 28.41], and $\mathbf{n}\bullet\mathbf{B}_2$ = +9.06; $\mathbf{B}_2$ has a component along **n**, and therefore this beam along $-\mathbf{B}_2$ is also directed downstream. A downstream directed beam on the flat-topped distribution is a characteristic of the Earth's bow shock [*Feldman et al.*, 1983a], but this is the first reported observation of such beams associated with interplanetary shocks.

2.3. Upstream Acceleration of Electrons

[9] The plasma line enhancements upstream of the shocks in Figure 2 indicate Langmuir plasma wave generation by electrons accelerated upstream by the interplanetary shock, similar to that observed in the electron foreshock upstream of the Earth's bow shock [*Feldman et al.*, 1983a]. The 26 August 1998 interplanetary shock was associated with a Type II radio burst and was first studied by *Bale et al.* [1999] who, using electron measurements from the Wind Three-Dimensional Plasma (3DP) experiment and WAVES/TNR experiment, detected velocity dispersed electron beams upstream of the shock simultaneously with the plasma waves, confirming that the upstream medium is a Type II burst source region. The velocity dispersion of the upstream electrons is due to the well-known time of flight effect that is a characteristic of the electron foreshock of Earth's bow shock (see the review by *Fitzenreiter* [1995]). A measurement by SWE/VEIS of a velocity distribution upstream of the 26 August 1998 interplanetary shock is shown in Figure 5. The lower panel is the reduced distribution $F(v_{\|})$, which is computed by integrating the contoured distribution $f(v_{\|}, v_{\perp})$ in the upper panel along vertical strips using the formula, $F(v_{\|}) = 2\pi \int v_{\perp} f(v_{\|}, v_{\perp}) dv_{\perp}$. The

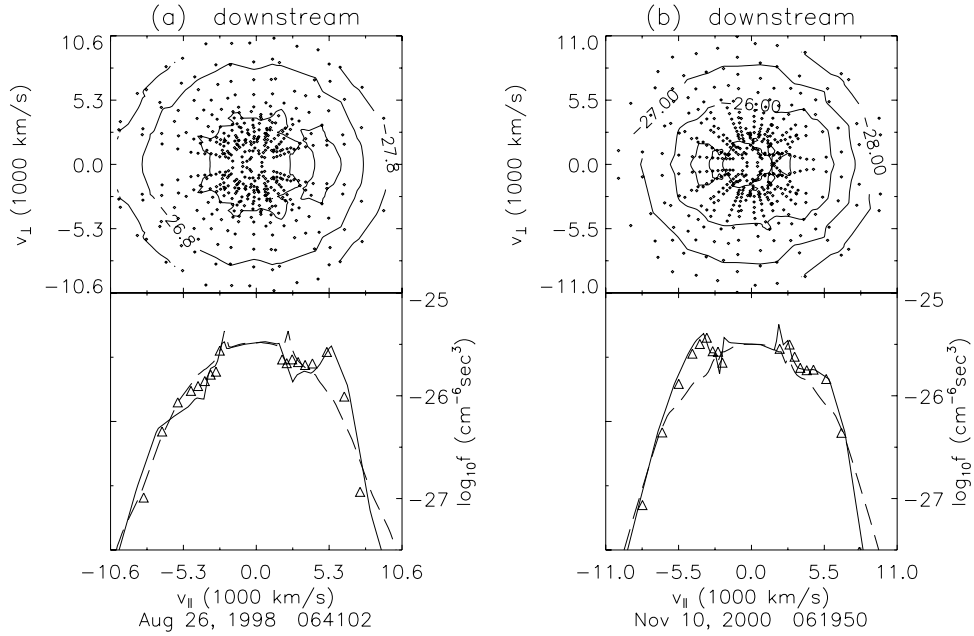

Figure 4. The velocity distributions downstream of the two shocks shown in Figures 3a and 3b on an expanded velocity scale in order to clearly show the beams on the shoulder of the flat-topped distributions. The beams are evident in the parallel cuts at $v_{||} = +5000$ km/s and $v_{||} = -5000$ km/s in the lower panels of Figures 4a and 4b, respectively, as well as by the corresponding closed contours in the upper panels.

vertical dashed line at $v_{||} = -4000$ km/s denotes the lower speed limit of the shock accelerated electrons that can be observed at the spacecraft location along magnetic field lines connected to the shock. The dashed line highlights the bump on the reduced distribution as well as the "notch" in the iso-f contours that turn upward for $v_{\perp} > 3000$ km/s, which indicates that the shock-induced enhancement in phase density extends over a wide range of pitch angles. Enhanced phase density with low speed cutoff at pitch angles outside the mirror loss-cone angle (35° in this case) as seen in Figure 5 is a signature of adiabatic mirror reflection of upstream electrons incident on the shock [*Leroy and Manganey*, 1984] and has been observed upstream of the Earth's bow shock [*Fitzenreiter et al.*, 1984, 1990]. The orientation of the magnetic field for the distribution shown in Figure 5 was such that measurements were not made within the mirror loss-cone as indicated by the absence of points underlying contours along the $-v_{||}$ direction. This means that energized electrons leaking upstream into the mirror loss-cone from the shock layer or through the shock from downstream were not measured by SWE/VEIS and thus do not contribute to the bump in computing the reduced distribution. The contours along this data gap have been determined by interpolation assuming the phase density at fixed electron speed is proportional to the square of the pitch angle. Enhanced electron flux antiparallel to the magnetic field and within the loss-cone was, however, measured for this event by the Wind 3DP experiment [*Bale et al.*, 1999]. In the analogous case of the Earth's bow shock, magnetic field-aligned upstream electron beams indicating leakage from the shock into the loss-cone have been observed by experiments on ISEE-1 and −2 [*Gosling et al.*, 1989]. Field-aligned beams upstream of the bow shock have also been observed by SWE/VEIS (when data sampling permits) simultaneously with the mirrored component (R. J. Fitzenreiter, unpublished manuscript, 1999). Although the bump on the reduced distribution shown in Figure 5 does not include a contribution from the leaking upstream component, the contribution from the mirrored component is substantial due to the $v_{\perp}$ - weighting of $f(v_{||}, v_{\perp})$ in the integrand used to compute $F(v_{||})$. In a previous study, the integrand $v_{\perp} f(v_{||}, v_{\perp})$ along the $v_{||}$ slice contributing to the bump on $F(v_{||})$has been shown to peak at $v_{\perp} > 0$ outside the mirror loss cone [*Fitzenreiter et al.*, 1984].

[10] The association of the plasma wave enhancements with the upstream electrons is shown in Figure 6 for the 26 August 1998 shock. The sequence of reduced distributions spanning the time interval over which wave enhancements occur are shown in the upper part of the figure. Each reduced distribution, $F(v_{||})$, was computed from $f(v_{||}, v_{\perp})$ as described above. The reduced distribution shown in Figure 5 is labeled "c" in Figure 6. The bump-on-tail distributions labeled "a," "b," "c," "d," "e," and "g" all coincide with enhancements in the electric field intensity, whereas the distribution labeled "f" has no bump-on-tail and coincides with relatively diminished electric field intensity. The reduced electron distribution data is plotted in the bottom panel as a contour map with time along the horizontal axis. The electrons accelerated upstream by the shock are evident in the figure as well as the downstream electron heating, which is indicated by the spreading apart of the iso-F contours.

[11] The *Bale et al.* [1999] study of the 26 August 1998 interplanetary shock inferred the existence and size of ripple-like protrusions on the shock based on the onset time

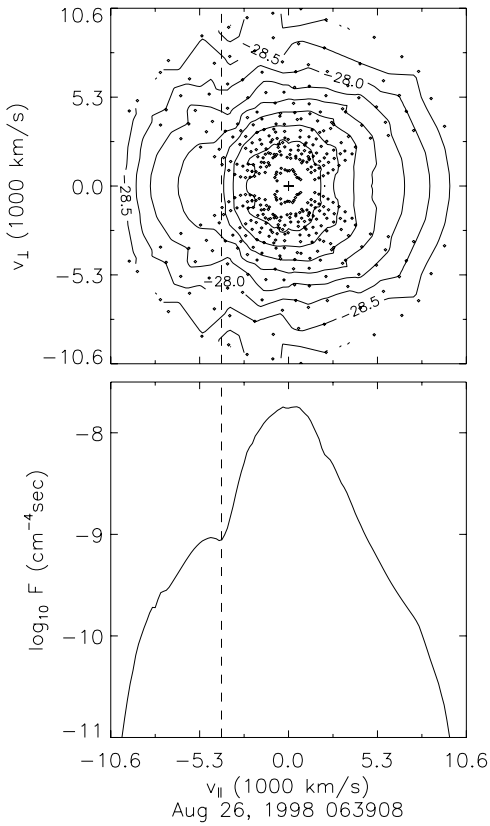

Figure 5. An electron velocity distribution observed upstream of the 26 August 1998 interplanetary shock which shows evidence of a shock-induced enhancement due to mirroring electrons moving back upstream. This is one of the upstream distributions that coincide with plasma wave enhancements associated with this shock. The vertical dashed line denotes the low velocity cutoff of the enhancement in the 2-D distribution in the upper panels as well as the bump on the reduced distribution function in the lower panel. The points underlying the contours are the velocity coordinates of the measurements. The contours close to the field direction where there are no measured points are an interpolation based on the data points closest to the magnetic field direction.

of the upstream waves prior to the shock arrival time. In order for a shock to efficiently energize electrons back upstream by magnetic mirroring, the magnetic field line must connect to the shock surface at a point where θ_{Bn} is close to 90° [*Leroy and Manganey*, 1984]. In the observational study by *Gosling et al.* [1989], the magnetic field-aligned beams of suprathermal electrons leaking upstream were always associated with nearly perpendicular crossings of the bow shock. In the case of the Earth's bow shock, a solar wind magnetic field line tangent to the curved shock surface ensures that $\theta_{Bn} \cong 90°$ at and near the point of magnetic field contact. In the case of an interplanetary shock, nominally assumed to be a planar surface, ripples on the surface probably provide points of magnetic field contact to the shock with $\theta_{Bn} \cong 90°$ allowing efficient energization of backstreaming electrons. Bale et al. deduced the rippled shock geometry consistent with their observations (see sketch in Figure 3, *Bale et al.* [1999]). According to the geometry in the sketch, how far upstream the protrusion extends determines how far upstream the shock accelerated electrons and plasma waves will be observed. Since the waves are observed 110s ahead of the shock, then the protrusion should extend 602 km/s × 110s = 6.6×10^4 km upstream, using the shock velocity, V_{shock}, from the R-H analysis. This result differs from the value, 13.7×10^4 km, obtained by Bale et al. The reason is that Bale et al. used the average shock speed based on the time when the shock left the Sun, whereas the instantaneous shock speed, which is lower in magnitude, was used here. Referring to Figure 2, plasma wave enhancements were observed upstream of the shocks occurring on 26 August 1998, 18 February 1999, and 15 May 1997, respectively. In the case of the 15 May 1997 shock, the upstream wave enhancements were only seen just before the shock crossing. Reduced velocity distributions (not shown) with a definite break are only seen in coincidence with the wave enhancements, consistent with shock-accelerated electrons having a time-of-flight low velocity cutoff. In this case, since the waves are observed only 35 s ahead of the shock, then the protruding structure should extend 417 km/s × 35s = 1.5×10^4 km upstream which is about one-fourth that of the 26 August 1998 shock. Variability such as this in the waves and accelerated electrons ahead of interplanetary shocks, i.e., how far ahead of the shock upstream effects are first seen, may provide information on the range of scale sizes of geometric irregularities on interplanetary shock surfaces.

3. Comparison of Liouville-Mapped and Observed Downstream Distributions

[12] The observed electron velocity distributions at the interplanetary shocks shown in Figures 3 and 4 show signatures of downstream electron heating, both parallel and perpendicular to the magnetic field, with downstream directed beams present in the strongest shocks. These characteristics are similar to electron signatures observed at the Earth's bow shock which have been explained by the macroscopic electric and magnetic fields in the shock layer acting on the adiabatic motion of the electrons [*Scudder*, 1995; *Hull et al.*, 1998, 2001]. In these studies, Liouville mapping was used, based on a solution of the Vlasov equation by the method of characteristics, which determines the distribution function at points between specified upstream and downstream boundaries, where the steady-state macroscopic fields are known, assuming the distribution function at one boundary is known. Our analysis follows the mapping, which *Hull et al.* [1998, 2001] applied at the Earth's bow shock. In this paper, we map an observed upstream distribution across an interplanetary shock and compare the result with the corresponding observed downstream distribution.

[13] We assume the interplanetary shock to be at rest with the upstream solar wind incident on the shock with the velocity $\mathbf{u} \bullet \mathbf{n} = \mathbf{u}_{sw} \bullet \mathbf{n} - v_{shock}$, where $\mathbf{u}$ is the solar wind velocity in the shock rest frame, $\mathbf{u}_{sw}$ is the solar wind velocity, $\mathbf{n}$ is the shock normal pointing in the upstream direction, and v_{shock} is the shock speed along $\mathbf{n}$. The mapping is done in the local deHoffman-Teller frame of reference (HTF), which is the simplest reference frame in

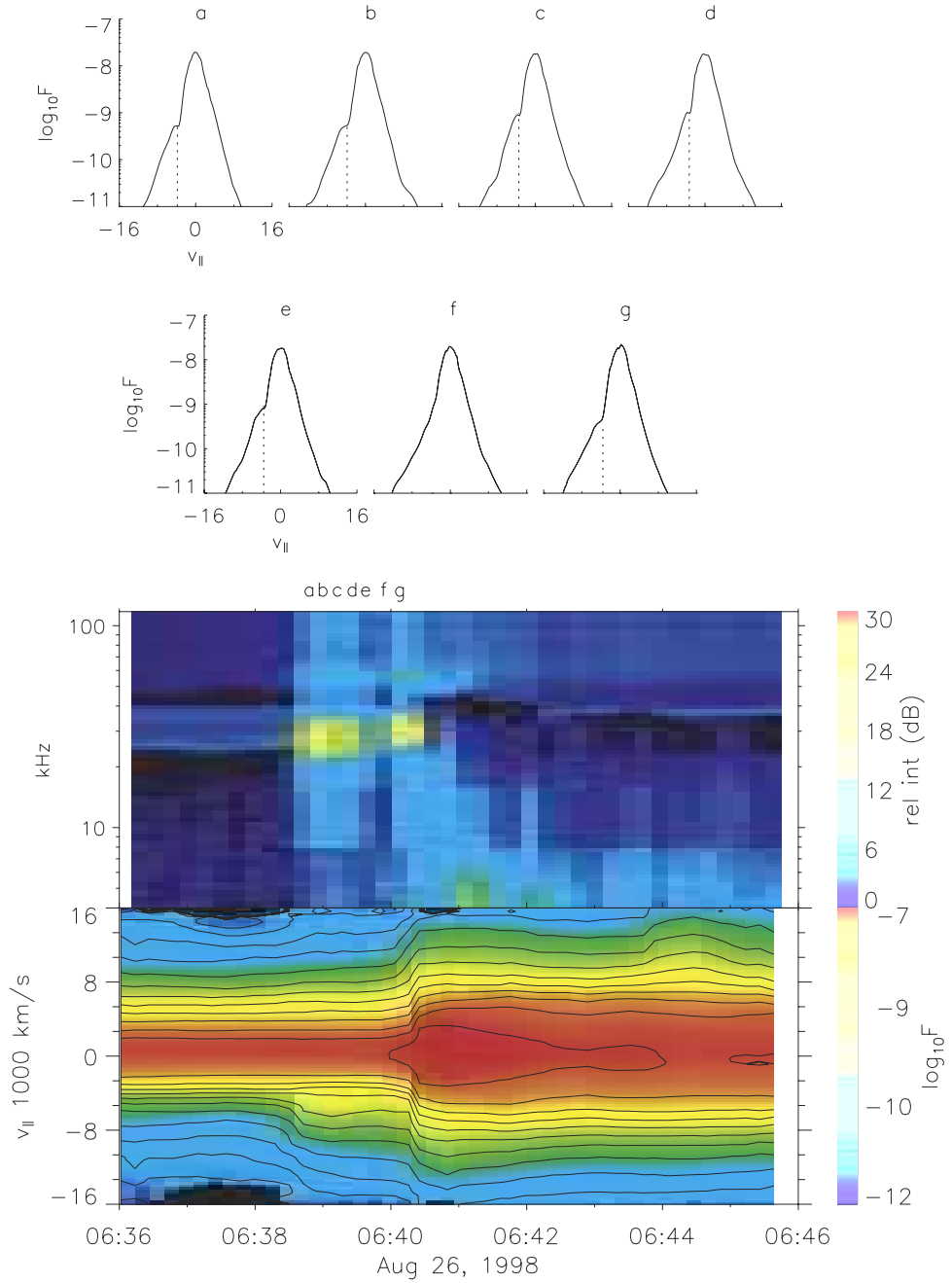

Figure 6. An overview of the association between the Langmuir wave enhancements in the upstream foreshock of the interplanetary shock, 26 August 1998, and the bump-on-tail reduced distributions, which generate the waves. The bottom two panels are the electric field fluctuations and a contour map of the reduced distribution across the shock with time on the horizontal axis, respectively. The reduced distributions in the upper part of the figure are time slices of the contour map in the upstream region, which is enhanced in phase density along $v_{\|} < 0$. Reduced distributions with vertical dotted lines at the time-of-flight velocity cutoff coincide with electric field enhancements seen in the second panel at the times denoted by a, b, c, d, e, and g, respectively. The units of reduced distribution F are cm^{-4} s and units of $v_{\|}$ are 1000 km/s.

which to consider the electron interaction because the electric potential is entirely along the normal. The velocity of the HTF in the rest frame of the solar wind incident on the shock with velocity **u** is given by

$$\mathbf{u}_{HT} = (\mathbf{n} \bullet \mathbf{u})/(\mathbf{n} \bullet \mathbf{b})\mathbf{b}, \quad (1)$$

where **b** is the magnetic field. The downstream electron distributions are constructed from the given upstream distribution by $f(v'_{2\|}, v'_{2\perp}) = f(v'_{1\|} - u_{ht}, v'_{1\perp})$, where $f(v'_{1\|} - u_{ht}, v'_{1\perp})$ is the given upstream distribution transformed to the HTF, and $f(v'_{2\|}, v'_{2\perp})$ is the mapped downstream phase density. The velocity space points $(v'_{1\|}, v'_{1\perp})$ and

Table 2. DeHoffman-Teller Potential Change Across the IP Shocks

Date, UT	$u_{ht\|\|}$ km/s	DTe eV	DQ eV	$D\phi_{ht}$ eV
26 Aug 1998 0640	−980	66	44	110
10 Nov 2000 0619	2310	82	2	84
18 Feb 1999 0249	−517	55	−16	39
6 Apr 2000 1627	−1250	52	6	58
21 Oct 1999 0213	−550	10	5	15
15 May 1997 0115	−1480	27	11	38

$(v'_{2\|}, v'_{2\perp})$ are the upstream and downstream points, respectively, that connect along velocity characteristics, which are the guiding-center trajectories of electrons having constant energy and magnetic moment. The velocity characteristics are given by

$$v'^2_{2\|} = (v''^2_{1\perp} - v'^2_{1\perp})(B_2/B_1 - 1) \quad (2)$$

$$v'^2_{2\perp} = v'^2_{1\perp}\,(B_2/B_1) \quad (3)$$

The velocity, $v''_{1\perp}$, is the upper bound of the perpendicular component of upstream velocity with access to the downstream and is given by

$$v'^2_{1\perp} \le v''^2_{1\perp} = \left[v'^2_{1\|} + 2e(\phi_2 - \phi_1)/m_e\right]/(B_2/B_1 - 1). \quad (4)$$

Equation (4) defines the mirror loss-cone, or more properly the focus-cone, since electrons moving from downstream to upstream are magnetically focused by the decrease in the magnetic field. However, we will follow the terminology used by Hull et al. and use the term loss-cone. The deHoffman-Teller potential change across the shock, $\phi_2 - \phi_1$, in equation (4) was computed from the SWE electron moments using the following expression derived from the steady state fluid electron energy equation by *Hull et al.* [2001],

$$\Delta[e\phi] = \Delta\left[\left(\frac{3}{2}\,kT_{e\|} + kT_{e\perp}\right) + q_\|/(u_{HT}N_e) + \frac{1}{2}m_e u^2_{HT}\right] \quad (5)$$

where N_e is the electron density, $T_{e\|}$ and $T_{e\perp}$ are the measured electron moment temperatures parallel and perpendicular to the magnetic field, respectively, $q_\|$ is the parallel electron heat flux, u_{HT} is the deHoffman-Teller velocity in the upstream using equation (1), and Δ refers to the difference between the downstream and upstream boundaries. Table 2 contains the quantities used in equation (5) for the shocks in this study. The table contains the value of u_{HT}, which remains constant, and the electron temperature and heat flux terms which change across the shock, where the table headings are DTe = 3/2 k($Te_{\|2}$ − $Te_{\|1}$) + k($Te_{\perp 2}$ − $Te_{\perp 1}$) and DQ = $q_{\|2}/(u_{HT}\ Ne_2)$ − $q_{\|1}/(u_{HT}\ Ne_1)$, and potential change, $D\phi_{HT} = \phi_2 - \phi_1$.

[14] The result of the mapping is shown in Figure 7 for the 10 November 2000 interplanetary shock. The observed distribution in Figure 7c serves as the boundary distribution, which is mapped to the downstream in Figure 7d. The upstream-to-downstream transformation in velocity space given in equations (2) and (3) is shown graphically in Figure 7a and 7b and shows the connecting upstream and downstream velocity space hemispheres in the HTF. Upstream phase space points in Figure 7a which map to the downstream in Figure 7b are shown in green, while downstream points in Figure 7b which map to the upstream in Figure 7a are shown in black. Note in Figure 7a and 7b that electrons crossing the shock upstream to downstream have $v'_\| > 0$ upstream but, as will be explained below, have $v'_\| < 0$ downstream, while electrons crossing in the opposite direction, downstream to upstream, have $v'_\| > 0$ downstream and $v'_\| < 0$ upstream. Because the mapping is reversible, the phase density for downstream electrons moving toward the shock, i.e., with $v'_\| > 0$, is determined from the upstream boundary distribution in the $v'_\| < 0$ hemisphere. The upstream velocity space with access to the downstream is bounded by the loss-cone separatrix (Figure 7a, computed from equation (4)). Electrons with velocity outside the separatrix mirror back upstream and are not included in this analysis. The empty elliptical downstream region centered on the origin (Figure 7b) is excluded from connection

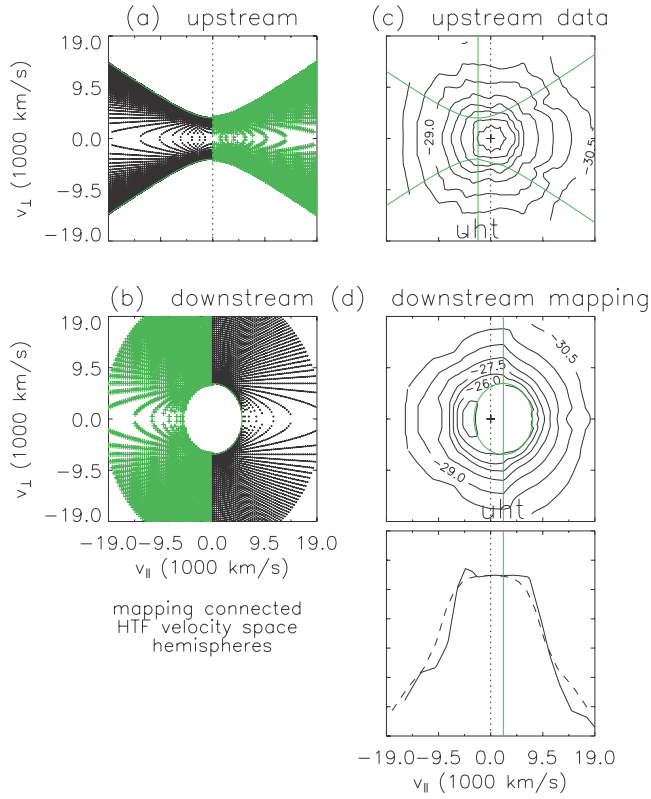

Figure 7. The result of the Liouville mapping analysis applied to the 10 November 2000 interplanetary shock. The velocity space mapping of connecting upstream and downstream hemispheres are shown in Figures 7a and 7b, with upstream to downstream connecting hemispheres shown in green, and downstream to upstream connecting hemispheres in black. The velocity transformation in Figures 7a and 7b is used to map the observed upstream distribution function (Figure 7c) to produce the downstream distribution (Figure 7d). The mapping is done in the HTF and the distributions are displayed here in the solar wind frame.

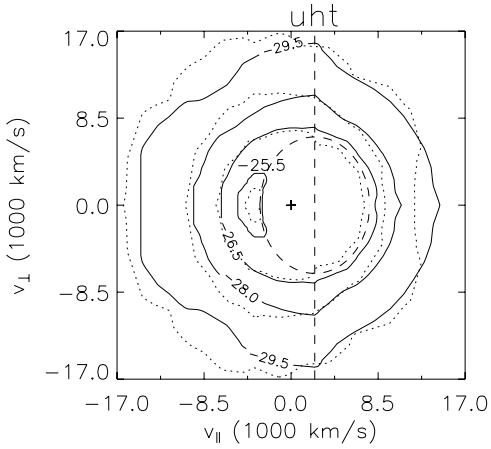

Figure 8. Comparison of the mapped distribution (solid contours) with the observed downstream distribution (dotted contours) for the 10 November shock event. The mapped and observed contours tend to overlap indicating that the mapping does a reasonably good job of reproducing the overall electron heating, as well as successfully reproducing the observed downstream beam.

to the upstream due to the increase in energy and pitch angle of electrons crossing upstream to downstream.

[15] The change in sign of $v'_{\|}$ for electrons crossing the shock is explained as follows: As required by the R-H shock analysis, the normal component of the magnetic field is continuous between the upstream and downstream asymptotic states. The shock analysis used the 92 s time resolution magnetic field and ion density and solar wind velocity measurements in 8-min intervals upstream and downstream to obtain the shock parameters. The 3 s electron measurements used for the mapping were not part of the asymptotic states but rather were data points adjacent to the shock layer. Although **b** ● **n** is continuous for the asymptotic state, **b** ● **n** changes sign between the 3 s intervals adjacent to the shock layer used in the mapping.

[16] Figure 7d is the result of mapping the observed upstream distribution in Figure 7c according to the point-to-point transformation of Figure 7a and 7b. The panel below the contour plot in Figure 7d shows cuts through the contours, the parallel (solid line) and perpendicular (dashed line). The deHoffman-Teller velocity, u_{HT} and the HTF loss-cone separatrix from Figure 7a are superposed as green traces on the upstream distribution of Figure 7c. In Figure 8, we compare the mapped distribution of Figure 7d with the distribution observed just downstream of the 10 November 2000 shock. The mapped and observed contours are the solid and dotted traces, respectively, using the same iso-f values for ease of comparison. The contour labels are values of log(f). The distributions are plotted in the solar wind frame, while the parallel velocity origin of the HTF, $v_{\|} = u_{HT}$, and the elliptical exclusion region are plotted as dashed traces.

[17] The mapped and the observed downstream distributions are in substantial agreement with respect to the following three signature characteristics:

[18] 1. On comparing the upstream distribution in Figure 7c with the mapped downstream distribution (solid trace) in Figure 7d, the mapped phase density contours downstream are inflated in both the perpendicular and parallel directions as a result of pitch angle broadening by the magnetic field jump and acceleration by the cross-shock potential. On comparing the mapped and observed distributions in Figure 8, note that the contours tend to overlap except for the contour, log(f) = −29.5, at $v_{\|} < 0$, indicating substantial quantitative agreement.

[19] 2. The thermal core of the upstream distribution has been accelerated, gaining energy in the parallel direction and broadened in pitch angle to form the beam indicated in Figure 8 by the closed contour, log(f) = −25.5, at $v_{\|} \sim -5000$ km/s just outside the elliptical separatrix bounding the exclusion region. Note that the observed beam (closed dotted contour) has a smaller parallel and perpendicular velocity width than the mapped beam (closed solid contour). This is probably due to scattering which would be necessary to redistribute and help fill in the elliptical exclusion region to which the beam is adjacent, as has been suggested for the bow shock beams [*Feldman et al.*, 1983a].

[20] 3. The mapped iso-f contours appear to be more widely separated for $v_{\|} < u_{HT}$, which correspond to electrons that have been transported upstream to downstream in the HTF, than for $v_{\|} > u_{HT}$, with an abrupt break in the contour shape at $v_{\|} \sim u_{HT}$. This break in the contour shape is also seen in the observed downstream distribution, as indicated by the overlap in the dotted and solid contours labeled log(f) = −28.0 in the vicinity of $v_{\|} \sim u_{HT}$.

[21] The 10 November 2000 event was selected for the mapping analysis because it is one of the strongest shocks in the set and because of the presence of the beam in the observed distribution. Because the deHoffman-Teller potential difference across the shock computed from equation (5) has the electron temperature increase as its dominant term, it is not surprising that there would be at least qualitative agreement in the overall inflated shape of the mapped distribution. However, the agreement of the relatively fine structure characteristics between the mapped and observed, such as the beam and the distribution shape in the vicinity of $v_{\|} \sim u_{HT}$, strongly supports the validity of the computed deHoffman-Teller potential and the mapping in the HTF. This shock was also selected for the mapping analysis because the magnetic field across the shock layer is monotonic with no overshoot, which means there are no trapped electron orbits within the elliptical exclusion region downstream. The *Hull et al.* [2001] mapping analysis shows that, in the magnetic overshoot case, the core of the upstream distribution is still accelerated to form the downstream beam just ahead of the exclusion region. We also applied the mapping to the 26 August 1998 interplanetary shock, which is a shock with a slight overshoot (see Figure 2), and reproduced the observed downstream shown in Figure 4a (the mapping for this case is not shown).

4. Summary and Conclusions

[22] Measurements of electron distribution functions at interplanetary shocks show that the electron distributions are modified both upstream and downstream of the shock.

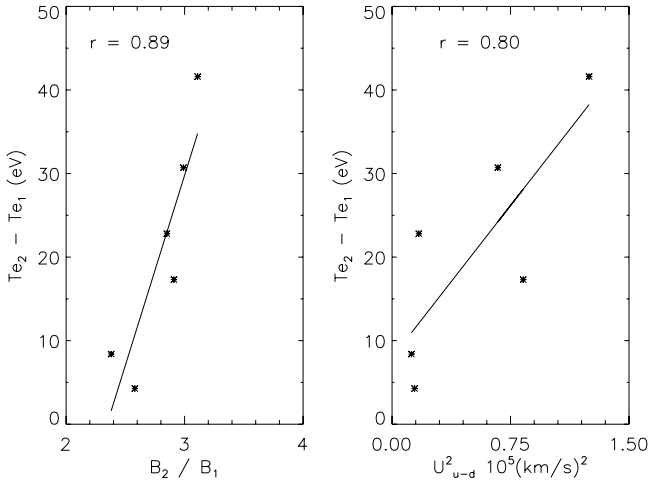

Figure 9. The electron temperature differences plotted as a function of the magnetic field ratio (Figure 9a) and the difference in the squares of the upstream and downstream solar wind speeds (Figure 9b), relative to the shock at rest, for all six interplanetary shocks in this study.

The shocks included in this study were all quasi-perpendicular, fast forward interplanetary shocks of moderate strength with electron density ratio, Ne_2/Ne_1 in the range 2.4 to 3.9. As the shock sweeps through the solar wind, the electron distribution function broadens downstream forming a flat-topped distribution indicating heating by the shock. Electron beams parallel to the magnetic field with energy approximately 75 eV also form downstream of the stronger shocks as observed at the bow shock of the Earth. Shock modified distributions are also observed upstream of the stronger shocks, with bump-on-tail reduced distributions which are coincident with plasma wave enhancements indicating Langmuir wave generation upstream. These shock-modified electron distributions are similar to electron distributions observed both downstream and upstream of the Earth's bow shock.

[23] We have applied a Liouville mapping analysis to one of the stronger shocks included in this study. The mapping technique follows closely the analysis of electron heating at the Earth's bow shock by *Hull et al.* [2001] and uses the de Hoffman-Teller electric potential computed from the observed electron moments using the steady state electron fluid energy equation. Upstream electrons within the mirror loss-cone map to the downstream and form the heating signature of the inflated distribution, both parallel and perpendicular with respect to the magnetic field direction, as well as the downstream low energy beam (see Figure 7). Comparison of the mapped and the observed distribution downstream in Figure 8 shows substantial quantitative agreement in the inflated iso-f contours, including the creation of the downstream beam. This agreement supports the assumption that the heating and acceleration signatures in distributions downstream of moderate strength interplanetary shocks can be explained to first order by adiabatic transport through the combined static electric and magnetic fields.

[24] A previous study of electron heating at interplanetary shocks by *Feldman et al.* [1983b, 1983c] has shown that for intermediate strength shocks, $Ne_2/Ne_1 > 2$ and flow velocity difference across the shock greater than 70 km/s, the electron temperature increase across the shock correlates with the difference between upstream and downstream bulk flow speeds. A study of heating at the Earth's bow shock by *Thomsen et al.* [1987] showed that the electron heating given by the temperature difference correlates best with the difference in the squares of upstream and downstream flow speeds, which is a measure of the available bulk flow energy. In Figure 9a and 9b, we plot the electron temperature difference as a function of both the magnetic field ratio, B_2/B_1 and the difference in the squares of upstream and downstream flow speeds (with respect to the shock), U^2_{u-d}. Although the number of samples is small, one can see by inspection that $Te_2 - Te_1$ is correlated to both B_2/B_1 and U^2_{u-d}, with the former correlation being somewhat better. *Hull et al.* [2000] found a positive linear relation between incremental changes in the de Hoffman-Teller electric potential, which is related to the temperature change, and incremental changes in the magnetic field through the shock layer and also provided an argument explaining the relationship. Because of the necessary zero current condition across the shock, electrons mirrored upstream outside the loss-cone by the magnetic field increase must be countered by an electric field accelerating electrons through the shock within the loss cone to the downstream.

[25] **Acknowledgments.** We thank M. L. Kaiser for providing the WAVES/TNR data and A. Szabo for providing MFI data at 3 s intervals. We also thank Matt Holland for assistance in developing the SDAT tool.

[26] Shadia Rifai Habbal thanks Jack Gosling and George C. Ho for their assistance in evaluating this paper.

References

Bale, S. D., M. J. Reiner, J.-L. Bougeret, M. L. Kaiser, S. Krucker, D. E. Larson, and R. P. Lin, The source region of an interplanetary type II radio burst, *Geophys. Res. Lett.*, *26*, 1573, 1999.

Bougeret, J.-L., et al., Waves, the radio and plasma wave investigation on the Wind spacecraft, *Space Sci. Rev.*, *71*, 231, 1995.

Feldman, W. C., S. J. Bame, S. P. Gary, J. T. Gosling, D. J. McComas, M. F. Thomsen, G. Paschmann, and M. M. Hoppe, Electron velocity distributions near the Earth's bow shock, *J. Geophys. Res.*, *88*, 96, 1983a.

Feldman, W. C., R. C. Anderson, S. J. Bame, S. P. Gary, J. T. Gosling, R. D. Zwickl, and E. J. Smith, Electron velocity distributions near interplanetary shocks, *J. Geophys. Res.*, *88*, 9949, 1983b.

Feldman, W. C., J. R. Asbridge, S. J. Bame, J. T. Gosling, and R. D. Zwickl, Electron heating at interplanetary shocks, in *Solar Wind 5*, edited by M. Neugebauer, *NASA Conf. Publ. CP-2280*, 403, 1983c.

Fitzenreiter, R. J., The electron foreshock, *Adv. Space Res.*, *15*, (8/9)9, 1995.

Fitzenreiter, R. J., A. J. Klimas, and J. D. Scudder, Detection of bump-on-tail reduced electron velocity distributions at the electron foreshock boundary, *Geophys. Res. Lett.*, *11*, 496, 1984.

Fitzenreiter, R. J., J. D. Scudder, and A. J. Klimas, Three-dimensional analytical model for the spatial variation of the foreshock electron distribution function: Sytematics and comparisons with ISEE observations, *J. Geophys. Res.*, *95*, 4155, 1990.

Goodrich, C. C., and J. D. Scudder, The adiabatic energy change of plasma electrons and the frame dependence of the cross shock potential at collisionless magnetosonic shock waves, *J. Geophys. Res.*, *89*, 6654, 1984.

Gosling, J. T., M. F. Thomsen, S. J. Bame, and C. T. Russell, Suprathermal electrons at the Earth's bow shock, *J. Geophys. Res.*, *94*, 10,011, 1989.

Hull, A. J., J. D. Scudder, L. A. Frank, W. R. Peterson, and M. G. Kivelson, Electron heating and phase space signatures at strong and weak quasi-perpendicular shocks, *J. Geophys. Res.*, *103*, 2041, 1998.

Hull, A. J., J. D. Scudder, R. J. Fitzenreiter, K. W. Ogilvie, J. A. Newbury, and C. T. Russell, Electron temperature and de Hoffman-Teller potential change across the Earth's bow shock: New results from ISEE-l, *J. Geophys. Res.*, *105*, 20,957, 2000.

Hull, A. J., J. D. Scudder, D. E. Larson, and R. P. Lin, Electron heating and phase space signatures at supercritical, fast mode shocks, *J. Geophys. Res.*, *106*, 15,711, 2001.

Lepping, R. P., M. H. Acuna, L. F. Burlaga, W. M. Farrell, and J. A. Slavin, The Wind magnetic field investigation, *Space Sci. Rev.*, *71*, 207, 1995.

Leroy, M., and A. Manganey, A theory of the energization of solar wind electrons by the Earth's bow shock, *Ann. Geophys.*, *2*, 4, 1984.

Ogilvie, K. W., et al., A comprehensive plasma instrument for the Wind spacecraft, *Space Sci. Rev.*, *71*, 55, 1995.

Scudder, J. D., A review of the physics of electron heating at collisionless shocks, *Adv. Space Res.*, *15*, (8/9)181, 1995.

Thomsen, M. F., M. M. Mellott, J. A. Stansberry, S. J. Bame, J. T. Gosling, and C. T. Russell, Strong electron heating at the Earth's bow shock, *J. Geophys. Res.*, *92*, 10,119, 1987.

Viñas, A. F., and J. D. Scudder, Fast and optimal solution to the Rankine Hugoniot Problem, *J. Geophys. Res.*, *91*, 39, 1986.

S. D. Bale, Space Sciences Laboratory, University of California, Berkeley, Berkeley, CA 94720, USA. (bale@ssl.berkeley.edu)

R. J. Fitzenreiter, K. W. Ogilvie, and A. F. Viñas, Laboratory for Extraterrestrial Physics, NASA Goddard Space Flight Center, Greenbelt, MD 20771, USA. (rfitzenreiter@msn.com; keith.ogilvie@gsfc.nasa.gov; vinas@unamuno.gsfc.nasa.gov)